DOI: 10.15480/882.9325

Eighth International Symposium on Marine Propulsors
smp'24, Berlin, Germany, March 2024

Prediction of the hydroacoustic emissions of a twin-screw vessel considering the phase angle of the propellers

Martin Scharf, Ulf Göttsche, Robert Beckmann, Raphael Bévand, Moustafa Abdel-Maksoud

Institute for Fluid Dynamics and Ship Theory, Hamburg University of Technology (TUHH), Hamburg, Germany

ABSTRACT

The propulsion system radiates a substantial fraction of the total sound energy, especially if sheet or vortex cavitation occurs. In this paper, a boundary element method is applied to investigate the sound propagation into the far field of a twin-screw vessel. It focuses on the effect of phase angle between the propellers on the sound levels. The flow simulations are conducted using a first order panel method to model the flow around the after ship. In addition, the Ffowcs Williams-Hawkings equation is used to predict the sound propagated into the far field. Sound levels in the far field as well as at distinct observation points are evaluated to gain an understanding of the mechanism.

Keywords

Underwater radiated noise (URN), boundary element method (BEM), Ffowcs Williams-Hawkings method (FWH), propeller cavitation

1 INTRODUCTION

Sound emissions from ships often fall within the frequency range that is important for marine life in terms of perception and communication (Duarte et al. 2021). The ship's propeller in conjunction with the cavitation phenomena, is usually the main source of noise. Regulations to reduce emissions from ships are beginning to take this aspect more and more into account, as in the latest guidelines published by the International Maritime Organisation (2023). Hydroacoustic emissions can be limited by focusing on them during the design process. For existing ships, design changes can only be implemented to a limited extent. In any case, modifications must be evaluated on their impact on the far-field sound pressure levels, as these affect marine life. In the present paper, different numerical methods are applied to simulate the flow around a propeller taking into account sheet cavitation and predict the resulting hydroacoustic emissions. The resulting pressure fields will be superposed and analyzed to gain insight into how the phase angle between the propellers of a catamaran influences its hydroacoustic radiation at different hydrophone locations. These phase angles may occur randomly or in a controlled way in reality, and while the presented method could be applicable to control the overall sound emissions, the focus in this contribution is on showing the effects of the phase angle on the spatial distribution of far field sound amplitudes.

2 METHODOLOGY

A potential flow based method is applied to model the propeller flow. The results are then processed by a Ffowcs Williams-Hawkings method to predict the sound pressure levels in the far field, which then are superposed to account for different phase angles of the propeller that were not modeled explicitly.

2.1 Flow Simulation

The applied flow simulation method is based on the potential flow theory, which is presented, for example, in Katz & Plotkin (2001). It describes an inviscid flow with an irrotational velocity field through the scalar velocity potential Φ:

$$\Delta\Phi = \nabla^2\Phi = 0. \tag{1}$$

Applying Greens second identity formulation on the Laplace equation in combination with the introduction of the inner potential Φ_I, source strength $\sigma = \frac{\partial\Phi_I}{\partial n} - \frac{\partial\Phi}{\partial n}$ and doublet strength $\mu = \Phi_I - \Phi$ leads to the following boundary value problem:

$$\begin{aligned} 0 = &- \frac{1}{4\pi}\int_{S_K} \vec{n}\cdot\left[\sigma\frac{1}{r} - \mu\frac{\partial}{\partial n}\frac{1}{r}\right]\mathrm{d}S \\ &- \frac{1}{4\pi}\int_{S_W} \vec{n}\cdot\left[\mu\frac{\partial}{\partial n}\frac{1}{r}\right]\mathrm{d}S \\ &+ \vec{v}_\infty(\vec{x}) + \vec{v}_{ext}(\vec{x}) \end{aligned} \tag{2}$$

that can be written in discretized form where the integrals

*

are replaced by sums over all elements on the respective surface. This is implemented in the panel code *pan*MARE that is actively developed at the Institute for Fluid Dynamics and Ship Theory and was first published in Hundemer (2010). The singularities of source and doublet strength and therefore also velocity and pressure are constant on each element. Sheet cavitation is modeled using a partially-nonlinear model based on Fine (1992) and Vaz (2005).

2.2 Acoustic Analogy

The Ffowcs Williams-Hawkings equation (Farassat & S. K. Brentner 1998) has been generalized from the Lighthill equation (Lighthill & Newman 1952)

$$\frac{\partial^2 \overbrace{\left(\rho u_i u_j + P_{i,j} - c^2 \rho' \delta_{i,j}\right)}^{=T_{i,j}}}{\partial x_i \partial x_j} = \frac{1}{c^2}\frac{\partial^2 p'}{\partial t^2} - \nabla p' \tag{3}$$

as follows by assuming the presence of solid bodies in the flow

$$\bar{\Box}^2 p' = \frac{\partial\left[\rho_0 v_n \delta\left(f\right)\right]}{\partial t} - \frac{\partial\left[l_i \delta\left(f\right)\right]}{\partial x_i} + \frac{\partial^2\left[T_{ij} H\left(f\right)\right]}{\partial x_i \partial x_j}, \tag{4}$$

where p' is the hydroacoustic pressure, ρ_0 the density of the undisturbed fluid, v_n the dot product of the motion velocity and surface normals $v_n = \vec{v}\cdot\vec{n}$, $\delta(f)$ the Dirac delta function of the distance f to the surface, T_{ij} the Lighthill turbulence stress tensor and $H(f)$ the Heaviside function.

The definition of a retarded time t_{ret} enables the evaluation of the source signal that contributes to the observed signal considering the wave travel time with the speed of sound c

$$t_{\text{ret}} = t^* - \frac{\left\|\vec{x}\left(t^*\right) - \vec{y}\left(t_{\text{ret}}\right)\right\|}{c} \tag{5}$$

the integral form was brought into the formulation 1 by K. S. Brentner & Farassat (2003):

$$\begin{aligned} 4\pi p'\left(\vec{x},t\right) =& \frac{1}{c}\frac{\partial}{\partial t}\int_{f=0}\left[\frac{\rho_0 c v_n + l_r}{r|1-M_r|}\right]_{\text{ret}} \mathrm{d}S \\ &+ \int_{f=0}\left[\frac{l_r}{r^2|1-M_r|}\right]_{\text{ret}} \mathrm{d}S \end{aligned}$$

$$p'\left(\vec{x},t^*\right) = p'_T\left(\vec{x},t^*\right) + p'_L\left(\vec{x},t^*\right) \tag{6}$$

with the terms for so-called thickness pressure p'_T and loading pressure p'_L:

$$\begin{aligned} p'_T\left(\vec{x},t^*\right) =& \frac{1}{4\pi}\int_S \left.\frac{\rho_0\left(\dot{v}_n + v_{\dot{n}}\right)}{r|1-M_r|^2}\right|_{\text{ret}} \mathrm{d}S \\ &+ \frac{1}{4\pi}\int_S \left.\frac{\rho_0 v_n\left(r\dot{M}_r + cM_r - cM^2\right)}{r^2|1-M_r|^3}\right|_{\text{ret}} \mathrm{d}S \end{aligned} \tag{7}$$

$$\begin{aligned} p'_L\left(\vec{x},t^*\right) =& \frac{1}{4\pi c}\int_S \left.\frac{\dot{l}_r}{r|1-M_r|^2}\right|_{\text{ret}} \mathrm{d}S \\ &+ \frac{1}{4\pi}\int_S \left.\frac{l_r - l_M}{r^2|1-M_r|^2}\right|_{\text{ret}} \mathrm{d}S \\ &+ \frac{1}{4\pi c}\int_S \left.\frac{l_r\left(r\dot{M}_r + cM_r - cM^2\right)}{r^2|1-M_r|^3}\right|_{\text{ret}} \mathrm{d}S \end{aligned} \tag{8}$$

This equation was then transformed into a discretized form by replacing the integrals with the sum across all panels on solid boundaries in the domain N_B in Göttsche (2020).

$$p'\left(\vec{x},t^*\right) = \sum_{i=0}^{N_B} p'_{T,i}\left(\vec{x},t^*\right) + p'_{L,i}\left(\vec{x},t^*\right) \tag{9}$$

For further details on the implementation and consideration of reflection at boundaries of the flow domain see Göttsche (2020).

2.3 Consideration of Phase Angle

The sound radiated by one half of the twin-screw vessel will be determined without any symmetry conditions or other consideration of the interaction between the two ship halves. The error introduced by this is inversely proportional to the distance between the propellers and assumed to be small in this case. The simulation yields the time history of sound pressure levels induced by the single propeller. The contribution of the other propeller at synchronous operation is simply the time dependent sound field mirrored at ship centerline. An arbitrary phase angle β at propeller rotation rate n is then taken into account through shifting the retarded time of the sound field mirrored at centerline by the equivalent time difference $\Delta T = \beta/n$.

3 TEST CASE

In order to evaluate the influence of phase angle on the far field sound pressure levels, a vessel with twin-screw configuration was considered. The test case *Princess Royal*, which has already been investigated in several publications (Aktas et al. 2015; Atlar et al. 2013; Brooker & Humphrey 2016; Carchen et al. 2015; Sampson et al. 2015; Shi et al. 2018; Turkmen et al. 2017) was selected. In the next subsections, the test case is described, followed by preliminary tests and the setup of the simulations.

3.1 Description

The *Princess Royal* is a catamaran with outward turning propellers on axes inclined by 8 degrees, described first in Atlar et al. (2013). A computer model rendering is shown in Figure 1.

Figure 1: Rendering of *Princess Royal* (Atlar et al. 2013)

Table 1: Particulars of the *Princess Royal*

Length	L_{oa}	18.88 m
Width	B	7.34 m
Width of single hull	B_h	2.44 m
Propeller diameter	D	0.75 m
Hub diameter ratio	d_h/D	0.16
Number of blades	z	5
Area ratio	A_e/A_0	1.057
Pitch ratio	$P_{0.7}/D$	0.8475

The main particulars of the vessel and its propellers are summarized in Table 1. Based on the operating conditions that have already been investigated in cited publications the one with the highest propeller loading was chosen, since it shows the highest extent of cavitation and is therefore numerically most challenging. The operating parameters are summarized in Table 2. The vapor pressure of water was set at 2500 Pa. A wake field published by Shi et al. (2018) was used for the propeller inflow (see Figure 2).

Table 2: Operating condition of the ship and propeller

Ship speed	v_s	$5.92\,\mathrm{m\,s^{-1}}$
Rotation rate	n	$14.25\,\mathrm{s^{-1}}$
Blade frequency	f_B	71.25 Hz
Hydrostatic pressure head	d_s	1.21 m
Thrust loading coefficient	c_{th}	2.36
Cavitation number	σ	0.19
Wake fraction	w	0.1304
Water depth	d	100 m

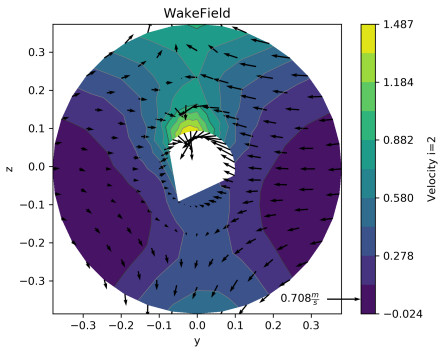

Figure 2: Wake field (Shi et al. 2018) (colored by external velocity component in axial direction)

3.2 Open water test

For validation of the panel method *pan*MARE in the behind condition the propeller, the hydrodynamic properties of the propeller were first calculated under open water conditions. Three different discretization levels were used to identify the adequate grid resolution for modeling the flow. The results are shown in Figure 3. The increase in error with decreasing advance coefficient is to be expected as the panel method is not capable to model the flow separation that occurs near the leading edge. According to the wake field used for the investigations and the wake fraction resulting from area weighted averaging, an equivalent advance coefficient was calculated, equal to

$$J = \frac{v_s(1-w)}{nD} = 0.48 \tag{10}$$

Although this operating condition is already in the region where the potential flow results start to show larger errors, these are still assumed to be small enough for the propeller loading to realistically represent the propeller load and cavitation patterns, see the comparison shown in section 4.

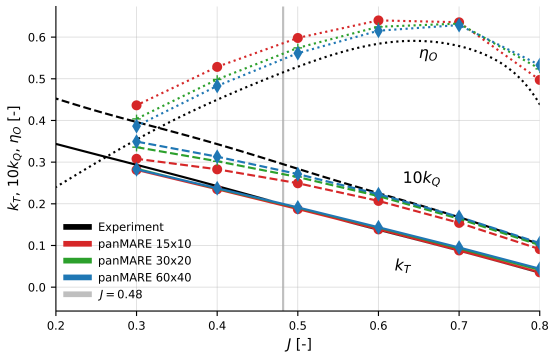

Figure 3: Open water diagram

3.3 Propeller behind hull

In order to reduce CPU time only the starboard side hull of the catamaran was included in the simulation. The interaction between both hulls was deemed to be negligible in terms of propeller operating conditions. The mesh shown in Figure 5 contains 6000 panels on the propeller blades and 2624 panels on the hull, which was only included up to 5.65 m forward of the stern. Viscous effects on the propeller inflow are modelled through the interpolation of the wake field from Shi et al. (2018). The resulting field is shown in Figure 4, the sampling points are marked. Although it later turned out that the port side propeller geometry was incorrectly used with the starboard wake field, the effect of propeller rotation direction on the far field sound levels is assumed to be negligible, as the axial component of the wake field of each hull is nearly symmetrical. For the material properties of the seabed, a density of $1746.6\,\mathrm{kg\,m^{-3}}$ and a sound speed of $1590.0\,\mathrm{m\,s^{-1}}$ were defined.

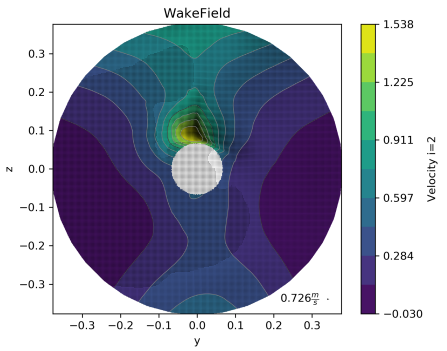

Figure 4: Wake field used in the simulation (evaluated in the propeller plane, colored by external velocity component in axial direction)

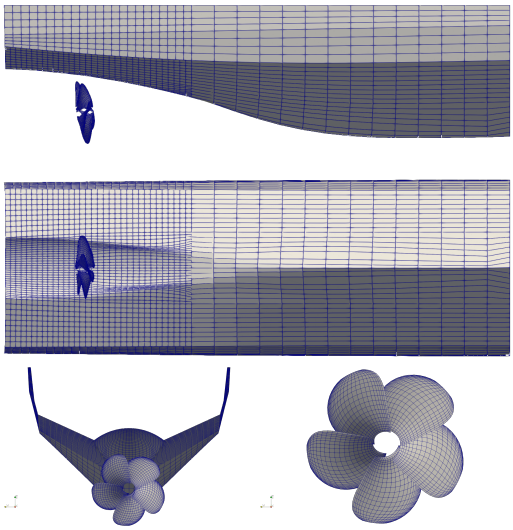

Figure 5: Panel mesh of aft hull and propeller

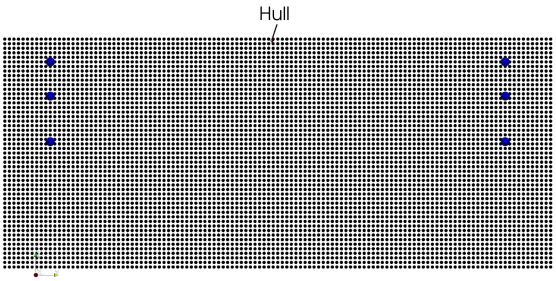

Figure 6: Axial plane in monitoring point field (hydrophone locations in blue)

Monitoring points are located at the six hydrophone locations 100 m off center line in water depths of 10, 25 and 45 m according to Brooker & Humphrey (2016). In order to gain a deep understanding into the sound pressure level distribution around the ship, 30855 points were distributed evenly on five transversal planes in a rectangular volume measuring 100 m in longitudinal direction, 240 m in horizontal direction and 100 m in vertical direction. The point locations on one of these planes is shown in Figure 6. For every single point in the pressure field the time signal of sound pressure was determined across the last four rotations of the propeller. The results were finally processed with FFT analysis resulting in a frequency spectrum for each point. A reference pressure of $p_{ref} = 1 \times 10^{-6}\,\mathrm{Pa}$ was used to convert the sound pressure levels to decibel.

4 RESULTS

Validation results for the FWH method with the same test case used here have already been presented in (Göttsche 2020). Therefore, this section focuses on the effect of the phase angle between both propellers on the far field sound pressure levels. Since the sheet cavitation fluctuations on the propeller blades are responsible for a significant part of the resulting far field sound pressure levels, they shall be presented first before analyzing the emitted sound. The sheet cavitation patterns obtained in the simulation and full scale observations, viewed from above the propeller, are shown in Figure 7. Bearing in mind that a comparison in this case can only be made qualitatively and that the camera position and perspective might not match completely, it can be seen that the calculated and measured results for the displayed propeller position are in good agreement. The numeric model was also able to predict the growth and collapse of the cavity sheet caused by the inclined axis as well as by the wake field that is expected during a blade revolution.

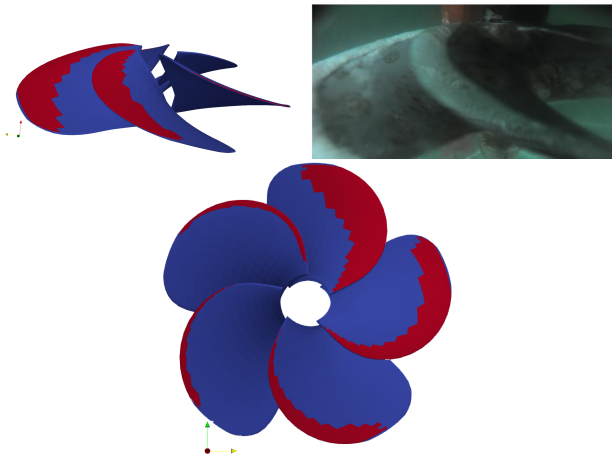

Figure 7: Cavitation pattern comparison between full scale observations from Turkmen et al. (2017) and the simulation

Analysis on the far field sound pressure amplitudes and the influence on phase angle thereon follows. In order to isolate the effect of phase angle for each monitoring point, a difference $\Delta\hat{a}$ in sound pressure level amplitudes relative to the reference value at zero phase angle was calculated and is shown in the following:

$$\Delta\hat{a} = \hat{a}(\beta) - \hat{a}(\beta = 0). \tag{11}$$

This term was evaluated at the first four harmonics of the blade passing frequency f_B. Firstly, the analysis will be presented for the six hydrophone locations, followed by a discussion of the results in the y-z plane passing through the propeller center for selected phase differences. Finally, an overview of results in the whole field of monitoring points is given.

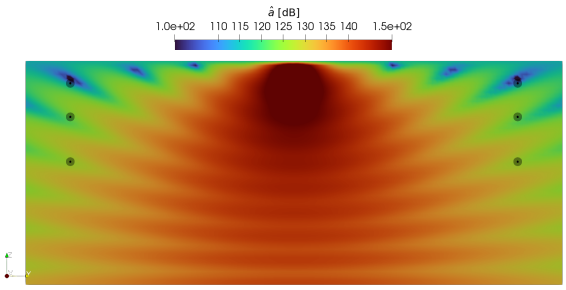

Figure 8: Pressure amplitudes for the sum of all paths in a y-z plane through the propeller center for first harmonic blade frequency

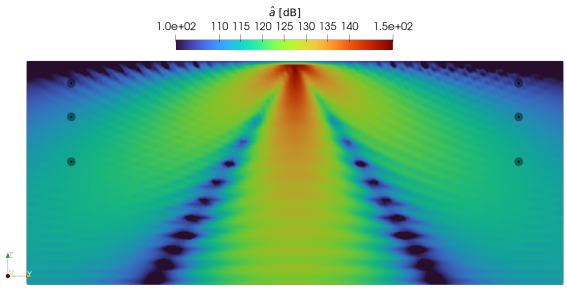

Figure 11: Pressure amplitudes for the sum of all paths in a y-z plane through the propeller center for $f = 4f_B$

Since it is the reference in $\Delta\hat{a}$ for the following investigations, the amplitudes of the sum of all sound paths for the first four blade harmonic frequencies are shown first. In Figure 8 the distribution of the first order amplitudes is presented. It is clear that the sound levels are the highest in the vicinity of the propeller and decrease with increasing distance, even more distinctively in transversal direction than in vertical direction. The visible pattern develops with the superposition of the results from the three different sound paths of the pressure wave to the monitoring point. These paths are the direct path, the reflection at the seabed and at the calm water surface. If not explicitly mentioned the behavior is described for the sum of all paths in the following. The superposition of signals causes already visibly differing values at the hydrophone locations. In Figures 9, 10 and 11 the amplitudes at higher harmonic frequencies are shown, each with an increasingly complex pattern due to the decreasing sound wave lengths.

The amplitude differences are visualized in Figures 12 for the direct path and in Figure 13 for the sum of all paths for the three hydrophone locations on each side of the vessel. The distributions of $\Delta\hat{a}$ show a number of extrema coinciding with the harmonic order of the evaluated frequency. It can be observed that there are relatively sharp minima of up to -30 dB with much wider maxima of +10 dB and higher in the results for the direct path as well as the sum of all paths. For the top two hydrophones, the increase in sound pressure amplitudes across all phase angles occurs only at the second and third blade harmonic frequencies. At fourth blade frequency the differences are negative across all phase angles for these hydrophones, but the phase angles of 18 and 54 degrees, where the local maxima are located in the second order graph, are still maxima. In all other frequencies at the three locations both increases and decreases were detected.

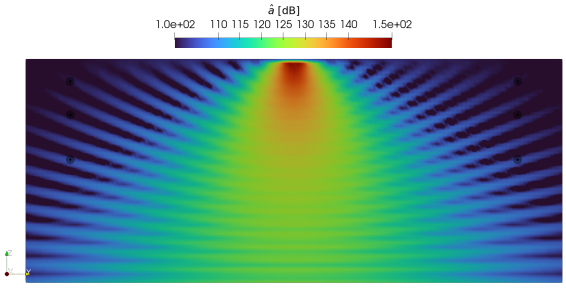

Figure 9: Pressure amplitudes for the sum of all paths in a y-z plane through the propeller center for $f = 2f_B$

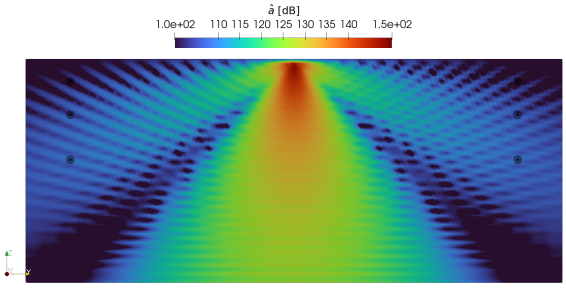

Figure 10: Sound level amplitudes for the sum of all paths in a y-z plane through the propeller center for $f = 3f_B$

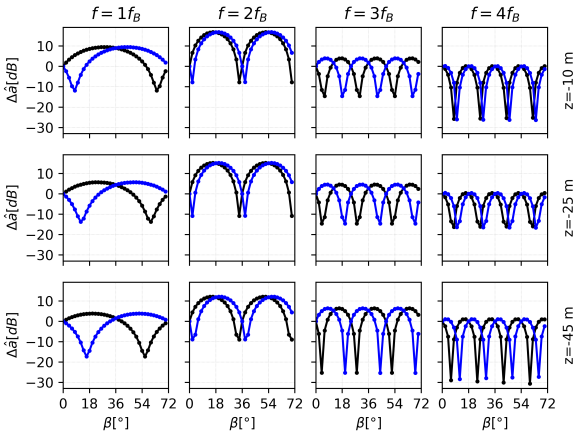

Figure 12: Influence of phase angle on pressure amplitudes of the direct path at the monitoring points (port side and starboard side, one depth per row as annotated on the right)

An effect similar to the phase shift can be observed with changing hydrophone depth. This is attributed to the fact that the hydrophones are not positioned on a straight line through the propeller axes, so that the propeller phase angle is not directly recognized as an equal phase change at each hydrophone in the signals.

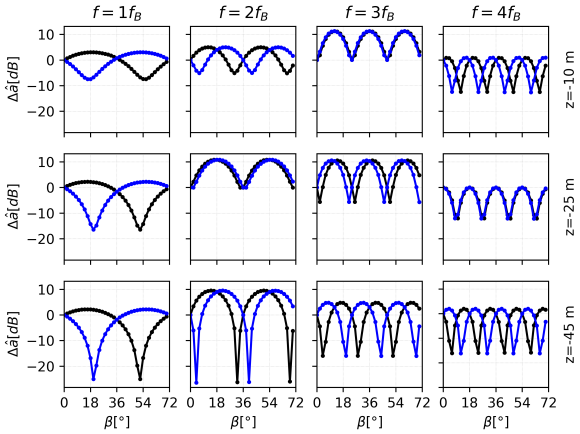

Figure 13: Influence of phase angle on pressure amplitudes of the sum of all paths at the monitoring points (port side and starboard side, one depth per row as annotated on the right)

In general, the results show an expected pattern of superposing sound wave amplitudes, with each curve of amplitude difference at a certain harmonic frequency showing as many minima. Since this gives insight on the effect of phase angle only at certain discrete locations, analysis on the influence on the spatial distribution of amplitudes follows.

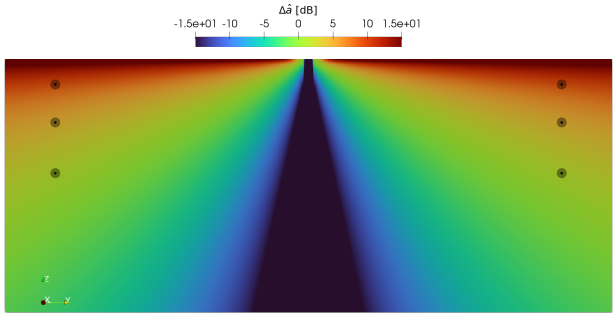

Figure 14: Sound pressure amplitude differences for the direct path ($\beta = 36°, f = f_B$)

The correlation between pressure amplitude difference and water depth becomes clear from the distribution of the levels of direct sound path in the y-z plane for a phase angle of $\beta = 36°$ (the half of the angle between two blades) at first blade harmonic in Figure 14. In a wedge-shaped area around ship center line the amplitudes are more than 15 dB lower than for synchronized propellers. The center plane is the only location where the distance of the signal or the equivalent retarded time is the same for both propellers while the signals are shifted by half a period, causing this negative interference. This difference increases into the positive range in transversal direction as well as in vertical direction for positions outside center line. The superposition of all paths in Figure 15 shows a more complex field because the reflections at the fluid boundaries cause each path to have slightly different retarded times at each point to begin with, which of course has a similar effect as a different phase angle between the two propellers for each path.

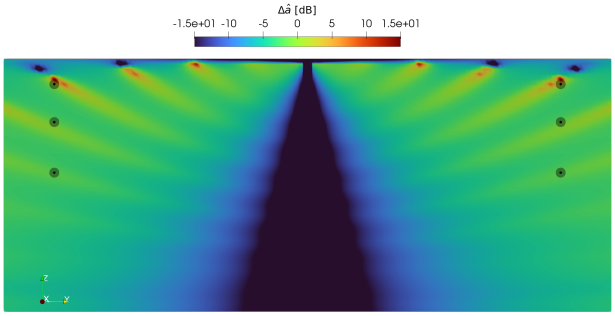

Figure 15: Sound pressure amplitude differences for the sum of all paths ($\beta = 36°, f = f_B$)

At second blade harmonic frequency, another particular effect can be observed. The amplitude field across the whole y-z plane does not change for a phase angle of 36 degrees, as shown in Figure 16. This is due to phase angle in this case being equal to the angle that the propellers rotate during the equivalent period of the harmonic sound wave. That means the configuration is completely synchronized regarding the second harmonic blade frequency and every even multiple of harmonic blade frequency as well.

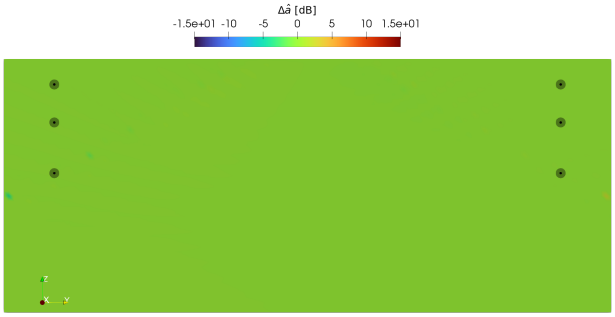

Figure 16: Sound pressure amplitude differences for the sum of all paths ($\beta = 36°, f = 2f_B$)

At other phase angles the amplitude difference is visible again, as already seen in the analysis of the results at the hydrophone locations. Compared to the distribution of amplitudes at first blade harmonic (see Figure 15) the amplitudes at second blade harmonic (see Figure 17) are showing more narrow area of lowered amplitudes directly below the propellers. Also, a pattern with more local detail develops. This qualitative behavior is in line with expectations since a sound wave at this frequency has a shorter wave length, leading to a decrease of the distances in space between areas of positive and negative interference. This nature appears even more clearly when comparing to a distribution at fifth blade harmonic (see Figure 18). Since the displayed phase angle in the latter case is not a multiple of the equivalent frequency the distribution is not symmetrical to the ship center line plane.

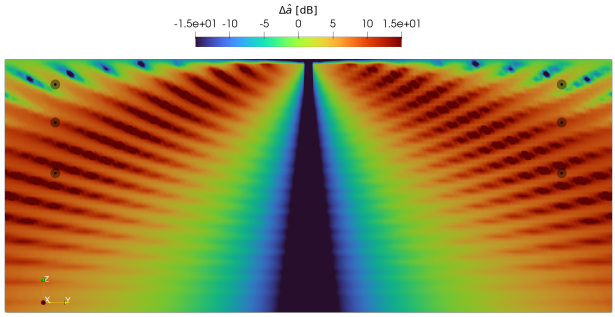

Figure 17: Sound pressure amplitude differences for the sum of all paths ($\beta = 18°$, $f = 2f_B$)

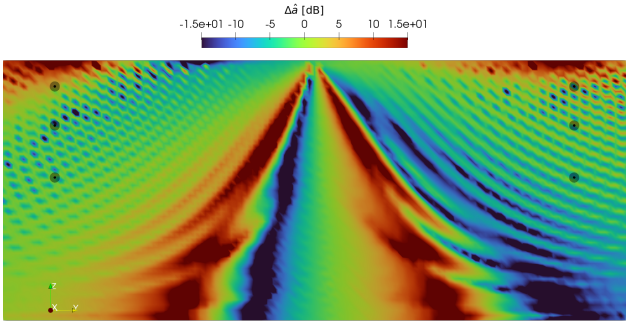

Figure 18: Sound pressure amplitude differences for the sum of all paths ($\beta = 18°$, $f = 5f_B$)

The distribution of the amplitudes at the first harmonic is also not necessarily symmetric, as displayed in Figure 19. The asymmetric distribution is not limited locally to the area around the hydrophones but extends to the whole domain. It can be observed that the noise levels on the starboard side are reduced, while they increase to a lesser extent on the port side.

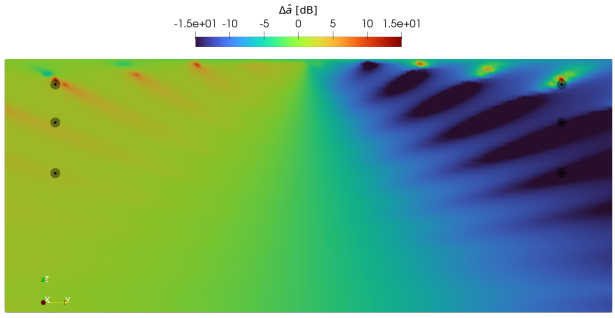

Figure 19: Sound pressure amplitude differences for the sum of all paths ($\beta = 54°$, $f = f_B$)

To quantify the presented change of amplitudes and show the effect in the whole monitored region, histograms of the pressure amplitudes for the available frequencies were generated for each investigated phase angle. The distributions for the phase angles 18 and 36 degrees are shown in Figure 20 and 21. Only those frequencies that had non-zero amplitude differences are included. The distributions in the range of lowered amplitudes extend further and exhibit a lower slope than on the side of increased amplitudes. Only the amplitudes at third harmonic show a clear increase in overall amplitude.

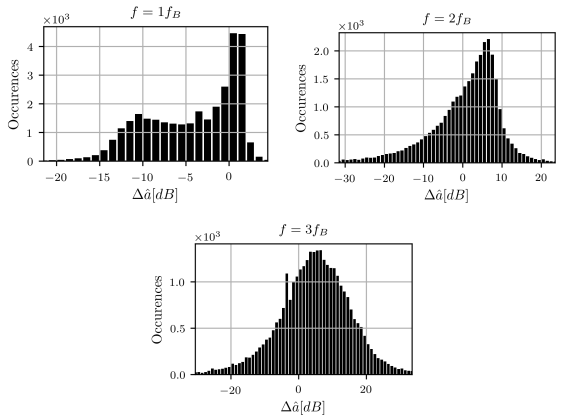

Figure 20: Histograms of the amplitude differences in sound pressure level at first and third harmonic frequency for the sum of all paths at $\beta = 18°$

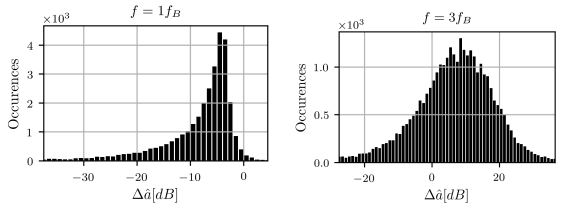

Figure 21: Histograms of the amplitude differences in sound pressure level at first and third blade harmonic frequency for the sum of all paths at $\beta = 36°$

As the aim in this study was not to minimize overall noise emissions, the analysis was not extended in this direction. For further investigations in this regard, it seems necessary to include a broader range of frequencies in the analysis than those considered in the present study. The sound level distributions presented lead to the conclusion that the phase angle in a twin-screw vessel should be taken into account when analyzing measurement or simulation results on noise emissions.

5 SUMMARY AND CONCLUSION

A boundary element method was applied to simulate the flow on the afterbody of one hull of a twin-screw catamaran. Based on the numerical results, the sound pressure levels in the far field were predicted using a FWH method. To take into account the contribution of the second propeller, the resulting sound level time series were superposed with the values at their symmetrical positions. Phase delay between the two propellers was introduced by delaying the time series of one propeller. The results were analyzed for a frequency of up to the fifth blade harmonic frequency.

The simulation method was able to predict a similar amount of sheet cavitation as reported in published experiments. A significant effect of the phase angle on sound level amplitudes was found for several hydrophone locations, with changes ranging between +10 dB and -30 dB. Distributions of the sound level amplitude difference

on planes in the simulation corresponds to the physically plausible expectation. Reduced sound levels were found in certain areas, e.g. below the keel for equivalent phase angles of half the respective period, while other areas showed increased amplitudes. This provides an indication that not only the number of measuring points should be carefully selected when assessing noise emissions, but also the phase angle should be taken into account for ships with more than one propeller.

A wider frequency domain needs to be investigated to quantify the potential of the reduction in noise emissions at properly controllable phase angles in twin-screw vessels.

6 ACKNOWLEDGEMENTS

The presented work was carried out as part of the German national research project MariData (http://maridata.org), which is funded by the German Ministry of Economic Affairs and Climate Action (BMWK) on the orders of the German Bundestag and PTJ as the conducting agency (FKZ 03SX528).

REFERENCES

Aktas, B. et al. (2015). "Underwater Radiated Noise Investigations of Cavitating Propellers Using Medium Size Cavitation Tunnel Tests and Full-Scale Trials". In: Fourth International Symposium on Marine Propulsors.

Atlar, M. et al. (2013). "A multi-purpose marine science and technology research vessel for full-scale observations and measurements". In: Proceedings of the 3rd International Conference on Advanced Model Measurement Technologies for the Marine Industry.

Brentner, K. S. & F. Farassat (2003). "Modeling aerodynamically generated sound of helicopter rotors". In: Progress in Aerospace Sciences 39.2, pp. 83–120.

Brooker, A. & V. Humphrey (2016). "Measurement of radiated underwater noise from a small research vessel in shallow water". In: Ocean Engineering 120, pp. 182–189.

Carchen, A. et al. (2015). "Design and Review of the new NPT Propeller for the Princess Royal". In: The 4th International Conference on Advanced Model Measurement Technology for the Maritime Industry (AMT15).

Duarte, C. M. et al. (2021). "The soundscape of the Anthropocene ocean". In: Science 371.6529, eaba4658. eprint: https://www.science.org/doi/pdf/10.1126/science.aba4658.

Farassat, F. & S. K. Brentner (1998). "The Acoustic Analogy and the Prediction of the Noise of Rotating Blades". In: Theoretical and Computational Fluid Dynamics 10.1, pp. 155–170.

Fine, N. E. (1992). "Nonlinear Analysis of Cavitating Propellers in Nonuniform Inflow". PhD thesis. Massachusetts Institute of Technology.

Göttsche, U. (2020). "Entwicklung einer numerischen Methode zur Vorhersage der hydroakustischen Schallabstrahlung von Schiffspropellern". PhD thesis. TU Hamburg.

Hundemer, J. (2010). "Entwicklung eines Verfahrens zur Berechnung der instationären potenzialtheoretischen Propellerumströmung". PhD thesis. TU Hamburg.

International Maritime Organisation (2023). *Revised Guidelines for the Reduction of Underwater Radiated Noise from Shipping to Address Adverse Impacts on Marine Life*. Tech. rep. International Maritime Organization.

Katz, J. & A. Plotkin (2001). *Low Speed Aerodynamics*. Cambridge University Press.

Lighthill, M. J. & M. H. A. Newman (1952). "On sound generated aerodynamically I. General theory". In: Proceedings of the Royal Society of London. Series A. - Mathematical and Physical Sciences 211.1107, pp. 564–587.

Sampson, R. et al. (2015). "On the full scale and model scale cavitation comparisons of a Deep-V catamaran research vessel". In: Fourth International Symposium on Marine Propulsors.

Shi, W. et al. (2018). "Stereoscopic PIV aided wake simulation of a catamaran research vessel using a dummy-hull model in a medium size cavitation tunnel". In: Journal of Marine Science and Technology 23, pp. 507–520.

Turkmen, S., M. Atlar, & N. Sasaki (2017). "Full-Scale Measurements of Underwater Radiated Noise of a Catamaran Research Vessel". In: Fifth International Symposium on Marine Propulsors.

Vaz, G. (2005). "Modelling of Sheet Cavitation on Hydrofoils and Marine Propellers using Boundary Element Methods". PhD thesis. Universidade Técnica de Lisboa.